Cement and Concrete Research 40 (2010) 171–178

Contents lists available at ScienceDirect

Cement and Concrete Research

journal homepage: http://ees.elsevier.com/CEMCON/default.asp

# Triaxial strength and failure criterion of plain high-strength and high-performance concrete before and after high temperatures

Zhen-jun He [a,*], Yu-pu Song [b]

[a] Department of Civil Engineering, Tsinghua University, Beijing 100084, China
[b] State Key Laboratory of Coastal and Offshore Engineering, Dalian University of Technology, Dalian 116024, China

ARTICLE INFO

*Article history:*
Received 29 March 2009
Accepted 27 August 2009

*Keywords:*
High-strength high-performace concrete (HSHPC) (E)
High temperatures (A)
Stress ratios (C)
Triaxial strengths (C)
Failure criterion (A)

ABSTRACT

Triaxial tests were performed on 100 mm × 100 mm × 100 mm cubic specimens of plain high-strength and high-performace concrete (HSHPC) at all kinds of stress ratios after exposure to normal and high temperatures of 20, 200, 300, 400, 500, and 600 °C, using a large static–dynamic true triaxial machine. Friction-reducing pads, using three layers of plastic membrane with glycerine were placed between the compressive loading plate and the specimens; the tensile loading planes of concrete samples were processed by an attrition machine, and then the samples were glued-up with the loading plate with structural glue. The failure mode characteristic of the specimens and the direction of the crack were observed and described. The three principally static strengths in the corresponding stress state were measured. The influence of the temperatures and stress ratios on the triaxial strengths of HSHPC after exposure to high temperatures was also analyzed. The experimental results showed that the uniaxial compressive strength of plain HSHPC after exposure to high temperatures does not decrease completely with the increase in temperature, the ratios of the triaxial to its uniaxial compressive strength are dependent on the brittleness–stiffness of HSHPC after different temperatures and the stress ratios. On this basis, a new failure criterion with the temperature parameters is proposed for plain HSHPC under multiaxial stress states. It provides the experimental and theoretical foundations for strength analysis of HSHPC structures subject to complex loads after subjected to a high temperature environment.



## 1. Introduction

Concrete has been the leading construction material for nearly a century. In recent years, high-performance concrete (HPC) is becoming an attractive alternative to traditional normal strength concrete (NSC). The alleged HPC is generally defined as high-strength, high fluidity, high durability concrete or to possess one of these performances; moreover, high-performance water reducer and superfine mineral admixtures are absolutely necessary ingredients. The dense microstructure of high-strength concrete (HSC) ensures high strength and very low permeability, so that it has a relatively low weak deformation capability or much higher "brittleness–stiffness" when compared to NSC. Recent fire test results show that there is a great difference between the properties of HSC and NSC after exposure to high temperatures [1–4]. It was observed that HSC is susceptible to spalling, or even explosive spalling when subjected to rapid temperature rise as in the case of a fire [5]. Hence, one of the main concerns for the usage of HSC in fire resistance applications is its performance under fire conditions. It is well known that the conventional analysis and design methods of reinforced concrete are generally still based upon material properties obtained from the basic uniaxial strength test, although we know that the true uniaxial condition in structures is extremely rare. In practice, many concrete structures such as shear wall, spiral columns and the node of building, nuclear reactor pressure container, etc are under multiaxial stress states. At the same time, with the wide use of computers, the finite element method and HSHPC in concrete structures, it has become increasingly evident that it is quite important and urgent for the experimental study on the mechanical property of HSHPC under multiaxial stress states, and for studies on the design and analysis of nonlinear behavior design of reinforced concrete structure based upon multiaxial mechanical behavior. So, many researchers have paid much attention to HSHPC at home and abroad. Late in the 1970s, some researchers [6] began to perform experimental study of "NSC" under multiaxial stress states in order to design for nuclear reactor container and so on. However, most studies [2,7] have been carried out to characterize the mechanical behavior of HSC or HPC under uniaxial stress state, or NSC under multiaxial stress states. Literature on the mechanical behavior of HSC or HPC under multiaxial loadings is extremely scarce; and, among them, most tests on confined compression (with two equal stresses) behavior of concrete have been performed under triaxial stress state using cylindrical specimens subjected to hydrostatic pressure in a triaxial cell and axial loading [8,9]. Lu and Thomas [9] studied the mechanical behavior of HSC and steel fiber reinforced high-strength concrete under uniaxial and triaxial compression, when testing $\Phi$ 100 mm × 200 mm and $\Phi$ 100 mm × 150 mm cylinder specimens

* Corresponding author.
*E-mail address:* zjhe@mail.tsinghua.edu.cn (Z. He).

0008-8846/$ – see front matter © 2009 Elsevier Ltd. All rights reserved.
doi:10.1016/j.cemconres.2009.08.024

**Table 1**
Mix proportions and major parameters of HSHPC.

| Strength levels | Water-cementitious ratio | Water ($kg/m^3$) | Cement ($kg/m^3$) | Fly ash ($kg/m^3$) | Fine aggregate ($kg/m^3$) | Coarse aggregate ($kg/m^3$) | Superplasticizer ($kg/m^3$) | Slump (cm) | Compressive strength ($f_C$/MPa) |
|---|---|---|---|---|---|---|---|---|---|
| HSHPC | 0.31 | 175 | 470 | 94.52 | 615.77 | 1094.71 | 6.77 | 24 | 60.16 |

lubricated with a combination of two 0.125 mm thick teflon sheets on top of one layer of a 0.015 mm thick aluminum foil. The previous investigations conducted on the effect of high temperatures on properties of plain HSC or HPC have also merely focused on the behavior of strength and deformation under uniaxial loading. However, literature on the mechanical properties of plain HSC or HPC under multiaxial stress states after high temperatures, has not been documented. Luo et al. [10] stated that the strength of the HPC degenerates more severely and has higher residual strength than that of NSC after exposure to high temperatures. Chan et al. [11] stated that the range between 400 °C and 800 °C is critical to the strength loss of concrete causing a large percentage of loss of strength. This paper presents the strength degradation rule and failure criterion of HSHPC at all kinds of stress ratios under triaxial stress states after exposure to six temperatures, using a large static–dynamic true triaxial machine. The triaxial tests were performed on 100 mm × 100 mm × 100 mm cubic concrete specimens. This paper may also serve as a reference (testing data, correlated formula and mechanical behavior) for the maintenance, design and the life prediction of HSC or HPC structure subjected to high temperatures , for example fire, etc.

## 2. Materials and experimental procedures

### 2.1. Materials and mix proportions

The cementitious materials used for this investigation were of Chinese standard P·I52.5R Portland cement (standard compressive strength higher than 52.5 MPa at the age of 28 days) and one-level fly ash [12,13]. The coarse aggregate was crushed stone (diameter ranging from 5 mm to 20 mm) and the fine aggregate was natural river sand (fineness modulus of 2.7); water was tap-water. Table 1 shows the mix proportions by weight of the mixture and the major parameters of HSHPC. ($f_C$ is the uniaxial compressive strength of 100 mm × 100 mm × 100 mm cubic HSHPC specimens with friction-reducing pads prior to high temperatures, and its strength value is about equal to that of 150 mm × 150 mm × 300 mm prism.).

### 2.2. Samples and testing methods

#### 2.2.1. Casting and curing of specimens

The coarse aggregate and fine aggregate were mixed for about 1 min when a portion of the proportional water was being sprayed on them, and then the cement and one-level fly ash were added in turn; after that, the residual proportional water with *SiKa$^{(R)}$NF-III* superplasticizer (these also obtain the abilities of increasing slump, durability and retardation besides ordinary water reducing agents.) was added slowly over a period of 1 min. Finally these ingredients were mixed for 2–3 min [13,14]. All specimens were cast in steel molds and compacted slightly by vibrating table, were demoulded after 24 h of the casting and then cured in a condition of 20 ± 3 °C and 95% RH (relative humidity) for 28 days according to "GBJ82-85 the test method of long-term and durability on ordinary concrete [15]", and then stored in a natural condition of 25 °C and 55% RH (relative humidity) in the room. The age of the specimens tested was about a year.

The concrete specimens tested were in 100 mm × 100 mm × 100 mm, 150 mm × 150 mm × 150 mm or 150 mm × 150 mm × 300 mm. The 100 mm concrete cubes were used to measure the strength for multiaxial tests. For determination of the strength classes for the HSHPC and the strength of the prism, each batch was cast in six 150 mm cubic specimens, and six 150 mm × 150 mm × 300 mm prismatic specimens.

#### 2.2.2. Apparatus and testing methods

The tests of high temperatures and multiaxial mechanical properties were performed at the State Key Laboratory of Coastal and Offshore Engineering, Dalian University of Technology. The high temperature testing apparatus and the multifunction triaxial experimental machine are shown in Figs. 1 and 2, respectively.

The specimens in high temperature test were 100 mm cubes. For each stress ratio, at least six specimens were heated. These 100 mm cubic specimens were heated to the peak temperatures of 200, 300, 400, 500, and 600 °C at a heating rate of 10 °C/min (the heating rate of 10 °C/min is referred to the furnace temperature.), respectively. After the peak temperature was reached, it was maintained for 6 h; the cooling time in electric furnace was about 1 h; then, the specimens were taken out and cooled naturally to room temperature. These specimens were tested in a multiaxial testing machine after 24 h. In this study, the surface of all specimens was dried before being exposed to high temperatures. No explosive spalling was observed during the high temperature tests on HSHPC specimens with temperatures ranging from 200 °C to 600 °C.

The triaxial tests were conducted in a triaxial testing machine that is capable of developing three independent compressive or tensile forces. The triaxial test process was necessary to insure uniform dimensions for each cubic specimen. The major stress direction was always applied perpendicularly to the surface of specimens. The proportional loading mode was employed. Friction-reducing pads placed between the platens and the specimens were three layers of plastic membrane with glycerine in-between for the compressive loading plane; the tensile loading plane of concrete sample was processed by an attrition machine, then, the samples were glued-up with the loading plate with structural glue. The specimens under triaxial compression were tested at a loading speed of 0.3–0.5 MPa/s in the direction of $\sigma_3$; but, those under uniaxial tension were done at 0.03–0.05 MPa/s in the direction of $\sigma_1$. Nine different stress ratios under triaxial compression loading after exposure to normal and high temperatures of 20, 200, 300, 400, 500, and 600 °C were tested. The principal stresses are expressed as $\sigma_1 \geq \sigma_2 \geq \sigma_3$ (compression denoted as negative and tension denoted as positive). For each specific stress ratio, at least three specimens were performed and their average values were used as the presented test results. During this process, results showing obvious deviation have been discarded. Fig. 3 shows

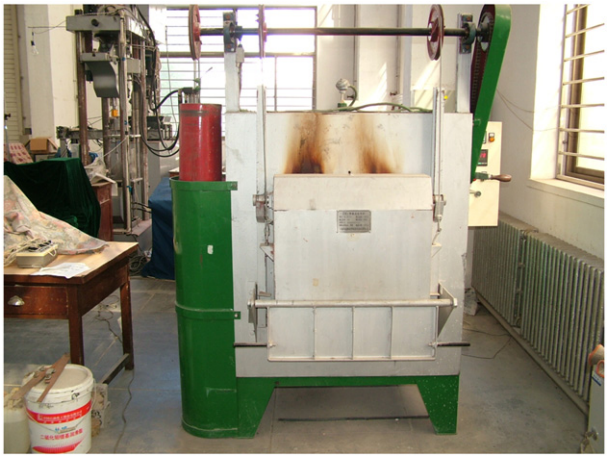

**Fig. 1.** The box-type electric furnace.

**Fig. 2.** The triaxial testing machine.

the loading direction and the states of the specimen under triaxial stress states in the triaxial experimental machine respectively.

## 3. Test results and discussions

### 3.1. Experimental results

The experimental results of plain HSHPC under triaxial stress states after high temperatures are given in Table 2.

### 3.2. Failure modes

The surface deterioration and the failure modes of the HSHPC specimens under multiaxial stress states subjected to the action of high temperatures are shown in Fig. 4(a–i).

From Fig. 4, it is obvious that the influence of high temperatures on HSHPC does not change the failure mode of tensile splitting. In Fig. 4(a, b), the HSHPC specimen under uniaxial compressive loading is split to multiple minor prisms (prism-type failure modes). As shown in Fig. 4(c, d), there are parallel plate-type fragments on the surface of $\sigma_2$ and $\sigma_3$ under biaxial compressive loading; moreover, the number of cracks becomes greater as the stress ratios and temperatures increase. They were the failure modes of the single-splitting cracks, single-shear and double-shear cracks of slant-shear shapes in random under triaxial compressive loading respectively, as shown in Fig. 4(e, f, g). It can also be seen that the single-shear and double-shear cracks of shear-type failure (the angle of the crack with the direction of $\sigma_3$ surface is about 20–30°) were formed on the surface of $\sigma_2$ under triaxial compression. The tensile failures under uniaxial tensile loading are shown in Fig. 4 (h, i), respectively. There was no connection between the direction of the cracking and stress ratios. It was noticed that the cracks on the loading surface have a random direction because of the influence of coarse aggregates.

The mentioned-above failure modes demonstrate that providing confinement stress along $\sigma_1$ and $\sigma_2$ directions will change the failure modes. Although the failure modes under triaxial stress states are different, the failure cause is that the splitting tensile strain along the unloading or less stress planes is greater than the ultimate tensile strain of the HSHPC.

### 3.3. Strength characteristics

As shown in Table 2 and Fig. 5, it is apparent that after 200 °C and 300 °C, the values of $-\sigma_{3f}/f_c$ are higher than 1 at the stress ratio of $\alpha=0$; that is, the corresponding uniaxial compressive strength $f_c^T$ is higher than $f_c$ (normal temperature), which is in disagreement with the conclusion on NSC and HSC in the references [16,17] respectively. But, when the suffered temperature is over 400 °C, it decreases gradually with the increase in temperature; this is in agreement with the conclusion on HSC in the reference [17]. As can be seen in Table 2

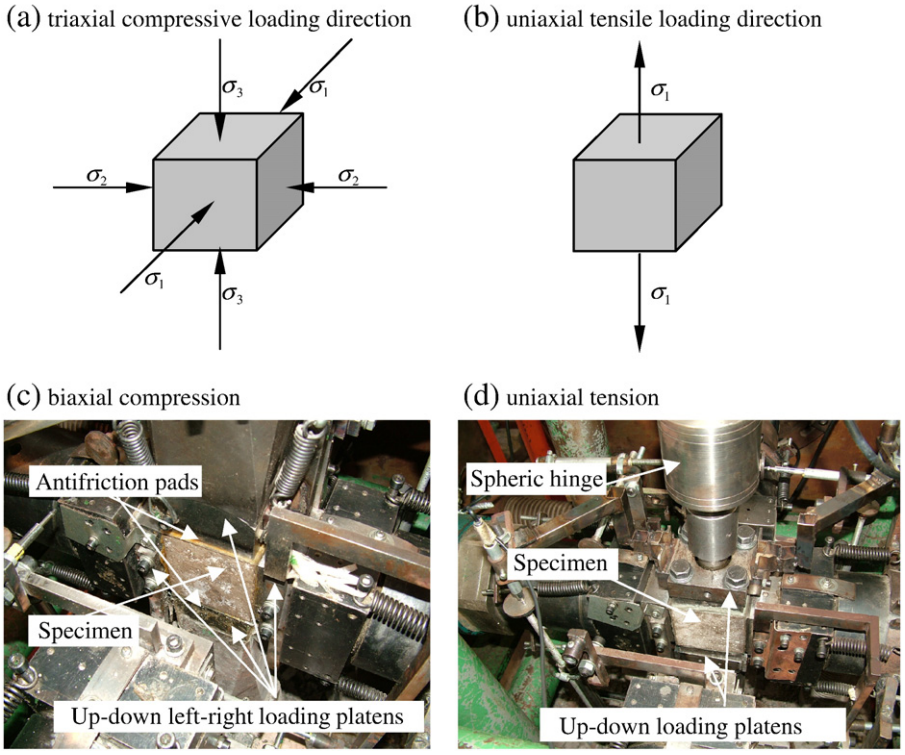


**Fig. 3.** States of the specimen in triaxial testing machine.

**Table 2**
The triaxial strength index of plain HSHPC under various stress states and stress ratios after high temperatures.

| Temperature levels/°C | Stress ratio $\alpha=\sigma_1:\sigma_2:\sigma_3$ | $\sigma_{1f}$/MPa | $\sigma_{2f}$/MPa | $\sigma_{3f}$/MPa | Temperature levels/°C | Stress ratio $\alpha=\sigma_1:\sigma_2:\sigma_3$ | $\sigma_{1f}$/MPa | $\sigma_{2f}$/MPa | $\sigma_{3f}$/MPa |
|---|---|---|---|---|---|---|---|---|---|
| 20 | 0.00:0.00:−1 | 0.00 | 0.00 | −60.16 | 400 | 0.00:0.00:−1 | 0.00 | 0.00 | −49.70 |
| | 1:0.00:0.00 | 5.08 | 0.00 | 0.00 | | 1:0.00:0.00 | 2.99 | 0.00 | 0.00 |
| | 0.00:−1.00:−1 | 0.00 | −66.78 | −66.78 | | 0.00:−1.00:−1 | 0.00 | −55.88 | −55.88 |
| | −0.10:−0.10:−1 | −12.03 | −12.03 | −120.28 | | −0.10:−0.10:−1 | −11.38 | −11.38 | −113.84 |
| | −0.10:−0.27:−1 | −14.36 | −38.78 | −143.63 | | −0.10:−0.27:−1 | −13.68 | −36.95 | −136.83 |
| | −0.10:−0.42:−1 | −15.34 | −64.43 | −153.40 | | −0.10:−0.42:−1 | −14.57 | −61.18 | −145.66 |
| | −0.10:−0.52:−1 | −15.77 | −82.03 | −157.74 | | −0.10:−0.52:−1 | −14.81 | −77.02 | −148.12 |
| | −0.10:−0.77:−1 | −15.25 | −117.45 | −152.53 | | −0.10:−0.77:−1 | −14.13 | −108.76 | −141.25 |
| | −0.10:−1.00:−1 | −13.16 | −131.64 | −131.64 | | −0.10:−1.00:−1 | −12.24 | −122.36 | −122.36 |
| 200 | 0.00:0.00:−1 | 0.00 | 0.00 | −63.96 | 500 | 0.00:0.00:−1 | 0.00 | 0.00 | −35.72 |
| | 1:0.00:0.00 | 4.81 | 0.00 | 0.00 | | 1:0.00:0.00 | 1.82 | 0.00 | 0.00 |
| | 0.00:−1.00:−1 | 0.00 | −67.48 | −67.48 | | 0.00:−1.00:−1 | 0.00 | −42.26 | −42.26 |
| | −0.10:−0.10:−1 | −12.10 | −12.10 | −121.00 | | −0.10:−0.10:−1 | −8.87 | −8.87 | −88.65 |
| | −0.10:−0.27:−1 | −14.77 | −39.89 | −147.74 | | −0.10:−0.27:−1 | −11.03 | −29.77 | −110.27 |
| | −0.10:−0.42:−1 | −15.01 | −63.05 | −150.11 | | −0.10:−0.42:−1 | −11.31 | −47.50 | −113.09 |
| | −0.10:−0.52:−1 | −15.53 | −80.76 | −155.31 | | −0.10:−0.52:−1 | −11.88 | −61.76 | −118.77 |
| | −0.10:−0.77:−1 | −14.60 | −112.42 | −146.00 | | −0.10:−0.77:−1 | −11.60 | −89.34 | −116.03 |
| | −0.10:−1.00:−1 | −12.38 | −123.78 | −123.78 | | −0.10:−1.00:−1 | −9.62 | −96.16 | −96.16 |
| 300 | 0.00:0.00:−1 | 0.00 | 0.00 | −61.64 | 600 | 0.00:0.00:−1 | 0.00 | 0.00 | −24.90 |
| | 1:0.00:0.00 | 4.14 | 0.00 | 0.00 | | 1:0.00:0.00 | 1.00 | 0.00 | 0.00 |
| | 0.00:−1.00:−1 | 0.00 | −66.69 | −66.69 | | 0.00:−1.00:−1 | 0.00 | −30.65 | −30.65 |
| | −0.10:−0.10:−1 | −12.30 | −12.30 | −123.00 | | −0.10:−0.10:−1 | −6.79 | −6.79 | −67.86 |
| | −0.10:−0.27:−1 | −13.89 | −37.49 | −145.85 | | −0.10:−0.27:−1 | −7.74 | −20.90 | −77.41 |
| | −0.10:−0.42:−1 | −16.05 | −67.41 | −160.50 | | −0.10:−0.42:−1 | −8.99 | −37.75 | −89.89 |
| | −0.10:−0.52:−1 | −15.69 | −81.60 | −156.92 | | −0.10:−0.52:−1 | −9.05 | −47.07 | −90.51 |
| | −0.10:−0.77:−1 | −15.41 | −118.63 | −154.07 | | −0.10:−0.77:−1 | −8.77 | −67.51 | −87.67 |
| | −0.10:−1.00:−1 | −12.82 | −128.22 | −128.22 | | −0.10:−1.00:−1 | −7.55 | −75.46 | −75.46 |

Note: $\sigma_{1f}$, $\sigma_{2f}$ and $\sigma_{3f}$ are the triaxial strengths in the three principal directions respectively.

and Fig. 5 (a, b), the uniaxial compressive strengths (63.96, 61.64, 49.7, 35.72, and 24.9 MPa) after being exposed to high temperatures of 200, 300, 400, 500, and 600 °C are 1.06, 1.02, 0.83, 0.59, and 0.41 times that of the original compressive strength at 20 °C (60.16 MPa) respectively; but, the uniaxial tensile strengths (4.81, 4.14, 2.99, 1.82, and 1.01 MPa) are 0.95, 0.82, 0.59, 0.36, and 0.20 times that of the original tensile strength(5.08 MPa) respectively. The above-mentioned discussion indicates that in comparison with the other temperatures, the uniaxial compression strength $f_c^T$ after 200 °Cand 300 °C is increased; but, the uniaxial tensile strength $f_t^T$ is gradually decreased with the increase in temperature. So, the temperatures around 400 °C are critical to the ultimate strength. ($f_c$, $f_c^T$ is the uniaxial compression strength with friction-reducing pads at normal temperature and after the other different temperatures, respectively).

It can be seen from Table 2, that the biaxial $\sigma_{3f}$ is higher than the corresponding $f_c^T$ at the stress ratio $\alpha=\sigma_2/\sigma_3=1$ for all temperatures. In addition, the influencing extent of the stress ratio on $-\sigma_{3f}/f_c^T$ is different with different temperatures. For example, when $\sigma_2/\sigma_3$ is equal to 1.00, the values of $-\sigma_{3f}$ (−66.78, −67.48, −66.69, −55.88, −42.26, and −30.65 MPa ) after being exposed to normal and high temperatures of 20, 200, 300, 400, 500, and 600 °C are 1.11, 1.12, 1.11, 0.93, 0.70, and 0.51 times that of the uniaxial compressive strength (60.16 MPa) prior to high temperatures respectively; but, they are 1.11, 1.06, 1.08, 1.12, 1.18, and 1.23 times that of the uniaxial strength (60.16, 63.96, 61.64, 49.7, 35.72, and 24.9 MPa) after the corresponding temperature respectively. Kupfer [18], Koya [19] and Mills and Zimmerman [20] performed biaxial concrete-strength tests. The results of the biaxial compressive strength tests of Kupfer and Helmut were about 1.18 to 1.27 times uniaxial compressive strength, when 200 mm × 200 mm × 50 mm plate specimens with brush-bearing platens as friction-reducing pads were used. The test results of Koya were about 1.25 to 1.40 times the uniaxial compressive strength when the maximum loading force was parallel with the direction of the cast, when testing 100 mm cubes with two resin sheets and silicon grease; the results of Mills and Zimmerman, using 57.4 mm cubes with two resin sheets and axle grease, were about 1.275 to 1.568 times the uniaxial compressive strength.

Fig. 6 (a) and (b) demonstrates the relationships between the middle stress ratio $\alpha=\sigma_2/\sigma_3$ and the ratios of the triaxial compressive strength $\sigma_{3f}$ to uniaxial compressive strength ($f_c$ and $f_c^T$) prior to and after high temperatures for HSHPC at different temperatures, respectively. It can be seen from Fig. 6(a) that the middle stress ratio $\alpha$ corresponding to the maximum strength $\sigma_{3f}$ is around $\alpha=0.50$. At the same temperatures, the change of $\sigma_{3f}$ is dependent on the stress ratio; moreover, the influence of the stress ratio on $\sigma_{3f}$ changes approximately by a parabolic-like curve. As shown in Fig. 6 (a), it is apparent that after 600 °C, the values of $-\sigma_{3f}/f_c$ are higher than 1 for all stress ratios. It can be seen from Fig. 6 (b) that the triaxial $\sigma_{3f}$ is much higher than the corresponding uniaxial compressive strength $f_c^T$ at the same temperatures for all stress ratios; in addition, the influencing extent of the stress ratio on $-\sigma_{3f}/f_c^T$ is different with different temperatures; moreover, the increasing extent of $-\sigma_{3f}/f_c^T$ under triaxial compression is much higher than that under biaxial compression. For example, when $\sigma_2/\sigma_3$ is equal to 0.42 or 0.52, the triaxial compressive strength is the greatest at every temperature; the values of $-\sigma_{3f}$ (−157.74, −155.31, −160.50, −148.12, −118.77, and −90.51 MPa ) after being exposed to normal and high temperatures of 20, 200, 300, 400, 500, and 600 °C are 2.62, 2.58, 2.67, 2.46, 1.97, and 1.50 times that of the uniaxial compressive strength (60.16 MPa) prior to high temperatures respectively; but, they are 2.62, 2.43, 2.60, 2.98, 3.33, and 3.63 times that of it (60.16, 63.96, 61.64, 49.7, 35.72, and 24.9 MPa) at the corresponding temperature, respectively. While, at normal temperature, the increasing percentage of $|-\sigma_{3f}/f_c|$ in this paper is less than that of the "NSC" in references [20–22], etc.

The above-mentioned discussion indicates that in comparison with the other temperatures, the uniaxial compression strength $f_c^T$ after 200 °C and 300 °C is increased; but, the ratio of $-\sigma_{3f}/f_c^T$ decreases; accordingly, its brittleness–stiffness of HSHPC is higher than that after the other high temperatures. So, the increasing extent of $-\sigma_{3f}/f_c^T$ under biaxial compression is dependent on the brittleness–stiffness of concrete after high temperatures besides the stress ratios. The greater the brittleness–stiffness of concrete after high temperatures, the less the increasing extent under biaxial compression. (Note: $f_c^T$ is the uniaxial compression strength with friction-reducing pads after different temperatures.).

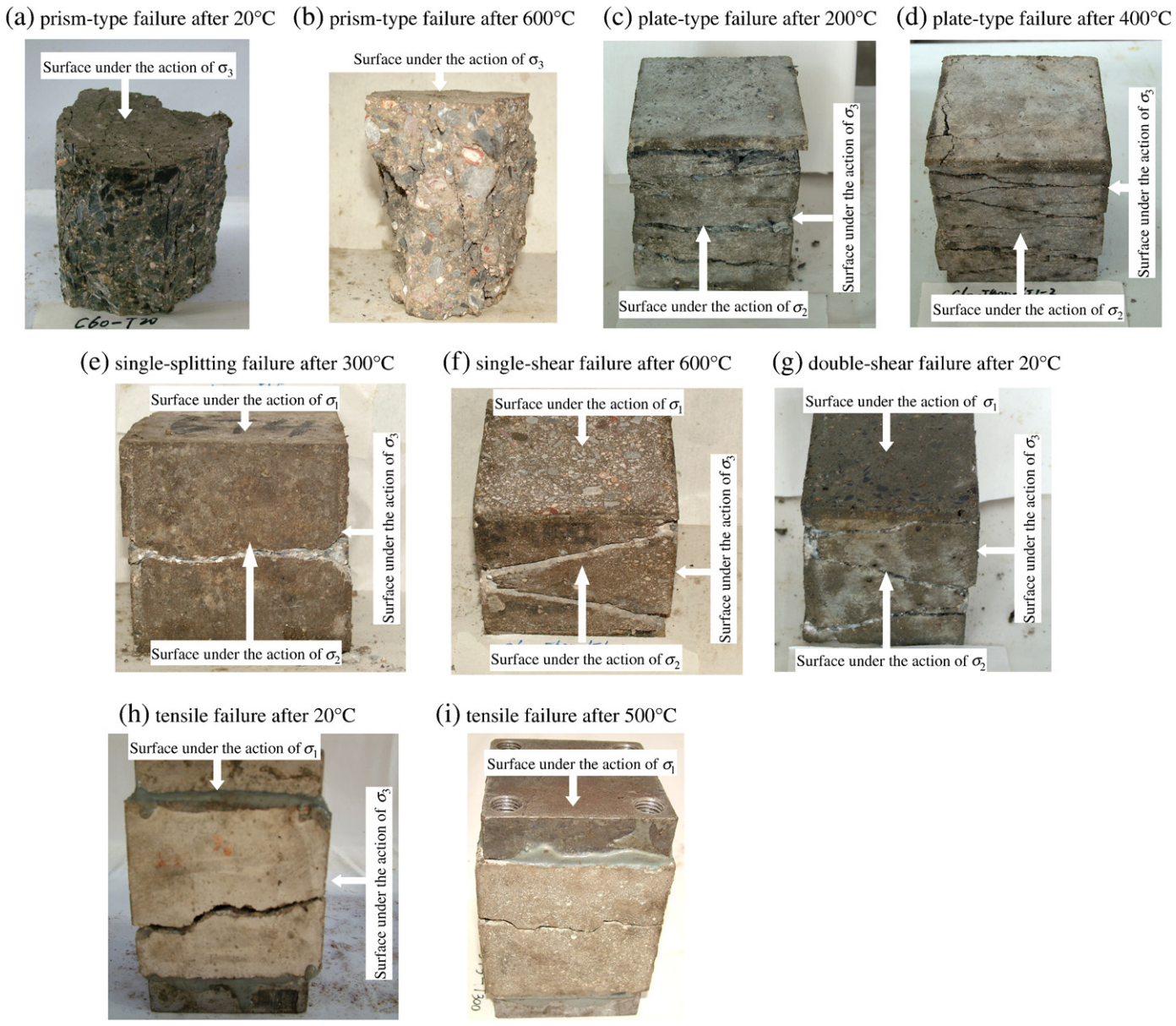


**Fig. 4.** Failure modes of plain HSHPC under multiaxial stress states at different temperatures.

So, through the above-mentioned discussion, it is indicated that the increasing extent of the multiaxial to uniaxial compressive strength is dependent on the stress ratios, stress states, and "brittleness–stiffness" of HSHPC after different temperatures, that the uniaxial compressive strength after exposure of up to 200 °C and 300 °C, is increased, and that their brittleness–stiffness is great, but, its extent of $-\sigma_{3f}/f_c^T$ is decreased. So, the increasing extent under multiaxial compression depends on the brittleness–stiffness of the concrete after exposure to different temperatures as well as the stress ratios. The greater the brittleness–stiffness of concrete after exposure to high temperatures, the less the increasing time under multiaxial compression. (The alleged "brittleness–stiffness" proposed in this paper is defined as "its strength of plain HSHPC is increased after different temperatures.").

### 3.4. Failure criterion

Based on the strength characteristic of experimental results in Table 2 and theoretical analysis of the failure enveloping plane, the present paper proposes a new failure criterion. The tensile-compressive meridians are proposed as follows:

$$\begin{aligned}\sigma_0^T &= a_1(\tau_{0t}^T)^2 + \lambda_1\tau_{0t}^T + c_1 \quad (\theta = 0^\circ)\\ \sigma_0^T &= a_2(\tau_{0c}^T)^2 + \lambda_2\tau_{0c}^T + c_2 \quad (\theta = 60^\circ)\end{aligned} \tag{1}$$

Where, $a_1, \lambda_1, c_1, a_2, \lambda_2, c_2$ are parameters which can be determined through the characteristics of the failure enveloping plane of concrete and experimental results in Table 2; $\sigma_{oct}^T$, $\tau_{oct}^T$, $\sigma_o^T$, and $\tau_o^T$ can be computed from:

$$\sigma_{oct}^T = \frac{\sigma_{1f}^T + \sigma_{2f}^T + \sigma_{3f}^T}{3} \quad \tau_{oct}^T = \frac{\sqrt{(\sigma_{1f}^T-\sigma_{2f}^T)^2 + (\sigma_{2f}^T-\sigma_{3f}^T)^2 + (\sigma_{3f}^T-\sigma_{1f}^T)^2}}{3} \tag{2}$$

$$\sigma_0^T = \frac{\sigma_{oct}^T}{f_c^T} \quad \tau_0^T = \frac{\tau_{oct}^T}{f_c^T} \tag{3}$$

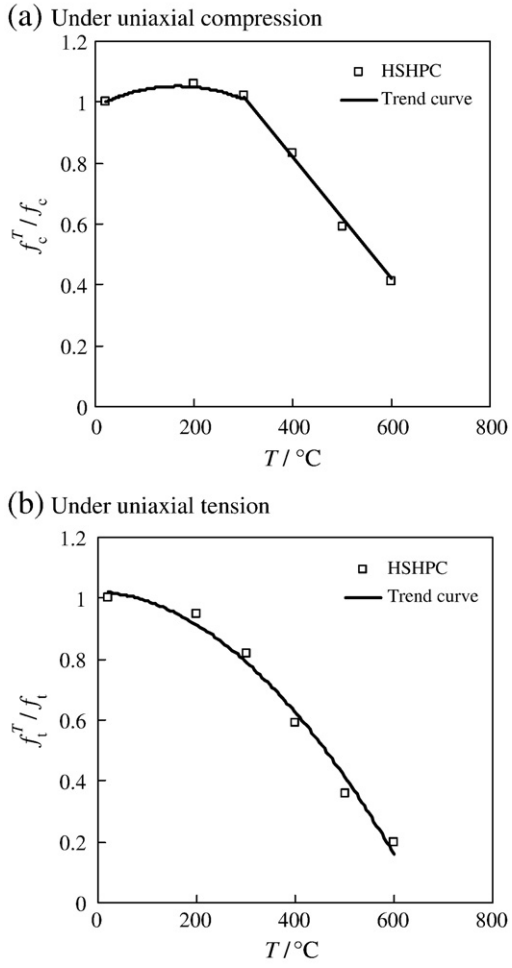


**Fig. 5.** The influence of the different temperatures on the $f_c^T/f_c$ and $f_t^T/f_t$ under uniaxial stress state.

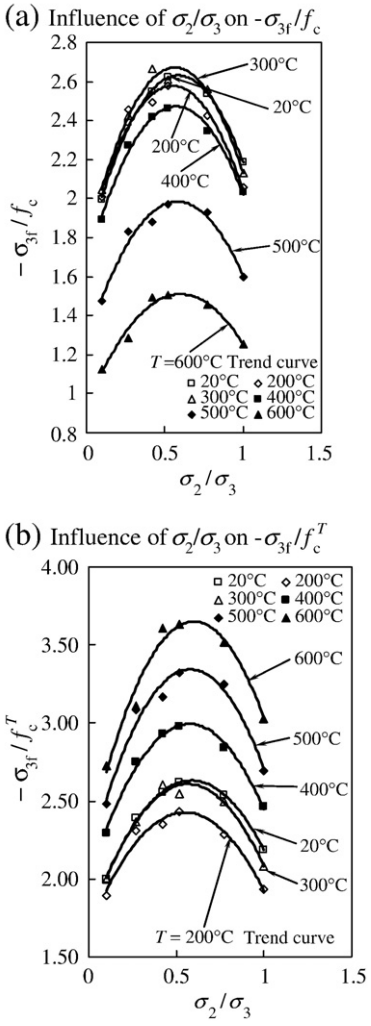


**Fig. 6.** The influence of the middle stress ratios on the principal stress $-\sigma_{3f}$ under triaxial compression at different temperatures.

where $\sigma_{oct}^T$ is octahedral normal stress; $\tau_{ot}^T$ and $\tau_{oc}^T$ are octahedral shear stress on tensile-compressive meridians for different temperatures respectively.

The parameters of tensile-compressive meridians are achieved by the characteristics of the failure enveloping plane of concrete as follows:

(1) Under equal tensile loading in the three directions (namely, $\tau_{ot}^T=\tau_{oc}^T=0$), the tensile-compressive meridians and hydrostatic stress axis converge in one point; that is,

$$c_1 = c_2 = \frac{\sigma_{ttt}^T}{f_c^T} = \frac{\sigma_t^T \times \eta^T}{f_c^T} \tag{4}$$

where $c$ is the ratios of the triaxial equal tensile strength to uniaxial compressive strength; that is, the values of crossing point coordinates between failure enveloping plane or tensile-compressive meridian and hydrostatic-pressure axis; $\sigma_t^T$ and $\sigma_{ttt}^T$ refer strength in uniaxial and triaxial tension respectively; $\eta^T$is proportionality coefficient between $\sigma_t^T$ and $\sigma_{ttt}^T$.

(2) The deviatoric plane turns into the shape of a circle($\gamma_c^T/\gamma_t^T=1$) gradually with the decrease of hydrostatic stress; that is,

$$\lim_{\xi^T\to-\infty}\frac{\gamma_t^T}{\gamma_c^T} = 1 \Rightarrow a_1 = a_2 \tag{5}$$

where $\xi^T$ is hydrostatic pressure; $\gamma^T$ is deviatoric stress; moreover, the maximum $\gamma_c^T$ and minimum $\gamma_t^T$ occurs at $\theta=60°$ and 0° respectively.

(3) The deviatoric plane is approximately triangle ($\gamma_t^T/\gamma_c^T=0.5$) when the hydrostatic stress reaches the maximum values gradually; that is,

$$\lim_{\xi^T\to 0}\frac{\gamma_t^T}{\gamma_c^T} \approx 0.5 \Rightarrow \lambda_1 \approx 2\lambda_2 \tag{6}$$

Eq. (1) is transformed into the following form.

$$\begin{aligned}\sigma_0^T &= a(\tau_{0t}^T)^2 + \lambda_1\tau_{0t}^T + c \ \ (\theta = 0^\circ)\\ \sigma_0^T &= a(\tau_{0c}^T)^2 + \lambda_2\tau_{0c}^T + c \ \ (\theta = 60^\circ)\end{aligned} \tag{7}$$

That is,

$$\sigma_0^T = a(\tau_0^T)^2 + \lambda\tau_0^T + c \ \ (0^\circ\le\theta\le 60^\circ) \tag{8}$$

Through repeated pilot calculation for strength values at different stress ratios of experimental results in Table 2, the equation of the deviatoric plane is given in the following form.

$$\lambda = \lambda_1(\cos 1.5\theta)^{1.35} + \lambda_2(\sin 1.5\theta)^2 \ \ (0^\circ\le\theta\le 60^\circ) \tag{9}$$

where $a$, $\lambda_1$, $\lambda_2$, and $c$ are the four parameters in the failure criterion that need to be empirically evaluated through the least square fit of the experimental data in Table 2 and Eq. (7). Determination of the four

**Table 3**
The parameter values of failure criterion for plain HSHPC after different temperatures.

| Temperature/°C | $a$ | $\lambda_1$ | $\lambda_2$ | $c$ |
|---|---|---|---|---|
| 20 | −0.4188 | −1.3530 | −0.6849 | 0.0826 |
| 200 | −0.5221 | −1.2968 | −0.6131 | 0.0717 |
| 300 | −0.4675 | −1.3021 | −0.6227 | 0.0641 |
| 400 | −0.3434 | −1.3435 | −0.6690 | 0.0584 |
| 500 | −0.3065 | −1.3322 | −0.6670 | 0.0492 |
| 600 | −0.2733 | −1.3226 | −0.6605 | 0.0388 |

parameters requires data pertaining to four different stress states. The present experimental program provided the data corresponding to four distinct stress states: uniaxial tension($\theta=0°$); uniaxial compression ($\theta=60°$); biaxial equal compression($\sigma_2=\sigma_3$, $\theta=0°$); and triaxial compression($\sigma_1=\sigma_2>\sigma_3$, $\theta=60°$). The calculated results in terms of the four parameters $a$, $\lambda_1$, $\lambda_2$, and $c$ are given in Table 3 at the different temperatures.

Using regression analysis of the parameter values in Table 3 for plain HSHPC after the different temperatures, the following formula is obtained (20 °C$\le T\le$600 °C):

$$\begin{cases} a = -7.6783\left(\frac{T}{1000}\right)^3 + 8.3336\left(\frac{T}{1000}\right)^2 - 2.0636\left(\frac{T}{1000}\right) - 0.3813 \quad (R^2 = 0.9816) \\ \lambda_1 = 3.2450\left(\frac{T}{1000}\right)^3 - 3.3163\left(\frac{T}{1000}\right)^2 + 0.9039\left(\frac{T}{1000}\right) - 1.3696 \quad (R^2 = 0.8821) \\ \lambda_2 = 3.8361\left(\frac{T}{1000}\right)^3 - 4.0407\left(\frac{T}{1000}\right)^2 + 1.1222\left(\frac{T}{1000}\right) - 0.7056 \quad (R^2 = 0.9406) \\ c = -0.0742\left(\frac{T}{1000}\right) + 0.0858 \quad (R^2 = 0.9875) \end{cases} \tag{10}$$

Fig. 7 gives the comparison of Eqs. (8)–(10) and test values. It can be seen from Fig. 7 that the model of failure envelopes in principal stress space for HSHPC under triaxial compression after being subjected to high temperatures, is of better precision and applicability.

## 4. Discussion

Concrete is a three-phase composite material at microscopic scale: a cementitious part, aggregate and the interfacial transition zones between the two. The micro-cracks will be formed due to drying and thermal shrinkage mismatch of aggregate particles and the cement part. The variation of temperature action can lead to the difference among the microstructures. The main reason for the change in the triaxial behavior of plain concrete after different temperatures was the formation and growth of micro-cracks during heat exposure. Micro-cracks mainly exist at cement paste-aggregate interfaces within the concrete even prior to any load and environmental effects. The slight increase in HSHPC strength associated with a further increase in temperature (between 200 °C and 300 °C ) is attributed to the general stiffening of the cement gel, or the increase in surface forces between gel particles, due to the removal of absorbed moisture. The temperature at which absorbed water is removed and the strength begins to increase depends on the porosity of the concrete. Above 400 °C, HSHPC loses their strength fast. At these temperatures, the dehydration of the cement paste results in its gradual disintegration which causes tension in the surrounding concrete. If the tensile stress exceeds the tensile strength of concrete, micro-cracks occur. The load carrying area will decrease with the initiation and growth of every new crack. On the other hand, considering the concrete specimen under compression with triaxial stress, the initiation and growth of every new crack will reduce the load carrying area. This reduction in load carrying area further causes an increase in the stress concentration at critical crack tips. So the compressive strength of plain concrete under compression with triaxial stress decreased with the increase of temperature. This effect is evidently observed over the temperature 400 °C. When the temperature is between 400 and 600 °C, $Ca(OH)_2$ decomposes; and above 600 °C , structural damage is influenced by $CaCO_3$ dissociation. This phenomenon occurs because the greater the damage is, the lesser compression the elements carry.

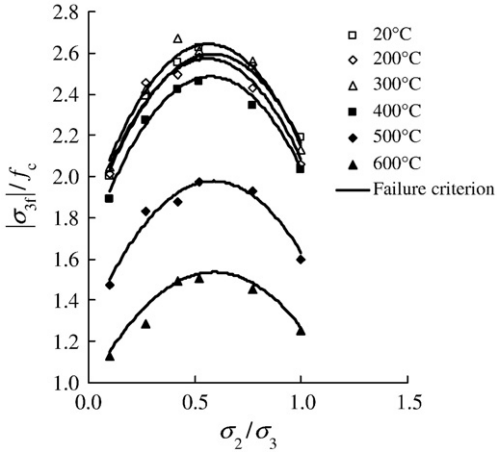


**Fig. 7.** The comparison of Eqs. (4) and (5) and test values under triaxial compression.

## 5. Conclusions

Based on the experimental work and the analysis of the test results, the following conclusions can be drawn:

(1) No explosive spalling is observed during the high temperature tests on the 100 mm cubic specimens for HSHPC with temperatures ranging from 200 °C to 600 °C.
(2) The effect of high temperatures on plain HSHPC does not change the failure modes. The failure modes of HSHPC prior to and after high temperatures under uniaxial, biaxial and triaxial compression are that of prism-type, parallel plate-type, and slant-shear shapes respectively; but, the failure modes under uniaxial tension are tension failure. The effect of confinement stress can change the failure modes.
(3) The ultimate strength $\sigma_{3f}$ of HSHPC under multiaxial compression for all stress ratios is higher than the corresponding uniaxial compressive strength for the same temperatures, especially under triaxial compression; but, the $\sigma_{3f}$ under biaxial tension-compression is less than it. The uniaxial compressive strength of plain HSHPC is not decreased after 200 and 300 °C. The brittleness–stiffness of HSHPC specimens between 200 °C and 300 °C is higher than that above 400 °C. The temperature around 400 °C is critical to the ultimate strength that decreases rapidly. The increasing extent of the triaxial to uniaxial compressive strength depends on the stress states, the stress ratios, and the brittleness–stiffness of HSHPC after different temperatures.
(4) A new failure criterion with the temperature parameters under multiaxial stress states is proposed for plain HSHPC.

## References

[1] Metin Husem, The effects of high temperature on compressive and flexural strengths of ordinary and high-performance concrete, Fire Safety Journal 41 (2) (2006) 155–163.
[2] Metin Husem, Serhat Gozutok, The effects of low temperature curing on the compressive strength of ordinary and high performance concrete, Construction and Building Materials 19 (1) (2005) 49–53.
[3] Min Li, Chunxiang Qian, Wei Sun, Mechanical properties of high-strength concrete after fire, Cement and Concrete Research 34 (6) (2004) 1001–1005.
[4] SammyY.N. Chan, Gaifei Peng, JohnK.W. Chan, Comparison between high strength concrete and normal strength concrete subjected to high temperature, Materials and Structures/Matdriaux et Constructions 29 (12) (1996) 616–619.
[5] Gaifei Peng, Wenwu Yang, Jie Zhao, et al., Explosive spalling and residual mechanical properties of fiber-toughened high-performance concrete subjected to high temperatures, Cement and Concrete Research 36 (4) (2006) 723–727.

[6] H. Kupfer, Behavior of concrete under biaxial stresses, ACI Journal 66 (8) (1969) 656–666.
[7] Sangkeun Lee, Youngchul Song, Sanghoon Han, Biaxial behavior of plain concrete of nuclear containment building, Nuclear Engineering and Design 227 (2) (2004) 143–153.
[8] Ahmad Mahboubi, Ali Ajorloo, Experimental study of the mechanical behavior of plastic concrete in triaxial compression, Cement and Concrete Research 5 (2) (2005) 412–419.
[9] Xiaobin Lu, Cheng-Tzu Thomas Hsu, Behavior of high strength concrete with and without steel fiber reinforcement in triaxial compression, Cement and Concrete Research 36 (9) (2006) 1679–1685.
[10] X. Luo, W. Sun, Y.N. Chan, Residual compressive strength and microstructure of high performance concrete after exposure to high temperature, Materials and Structures/Materiaux et Constructions 33 (6) (2000) 294–298.
[11] SammyY.N. Chan, Gaifei Peng, JohnK.W. Chan, Comparison between high strength concrete and normal strength concrete subjected to high temperature, Materials and Structures/Matdriaux et Constructions 29 (12) (1996) 616–619.
[12] The National Standards Compilation Group of the People's Republic of China, GB175-1999 Portland Cement and Ordinary Portland Cement, China Standards Press, Beijing, 1999 (in Chinese).
[13] The High-strength High-performance Concrete Committee of China Civil Engineering Society, Guide for structural design and construction of high-strength concrete, China Architecture and Building Press, Beijing, 2001 (in Chinese).
[14] The National Standards Compilation Group of the People's Republic of China, GB/T 50081-2002 Standard for Test Method of Mechanical Properties on Ordinary Concrete, China Architecture and Building Press, Beijing, 2003 (in Chinese).
[15] The National Standards Compilation Group of the People's Republic of China, GBJ82-85 Testing Methods of Long-Term and Long-Lasting Performance of Ordinary Concrete, China Architecture and Building Press, Beijing, 1985 (in Chinese).
[16] Likun Qin, Yupu Song, Zhong Zhang, et al., The research on strength and deformation of plain concrete under biaxial compression after high temperatures, Journal of Dalian University of Technology 45 (1) (2005) 113–117 (in Chinese).
[17] Wu Bo, Yuan Jie, Wang Guang-yuan. Experimental research on the mechanical properties of HSC after high temperature. China civil engineering journal, 2000, 33 (2): 8–12, 34.
[18] H. Kuper, K.H. Gerstle, Behavior of concrete under biaxial stresses, ASCE 99 (EM4) (1973) 853–866.
[19] Koya, et al., Strength of concrete under biaxial compressive loading, Cement and Concrete 322 (Dec. 1973) 17–23 (in Japanese).
[20] L.L. Mills, R.M. Zimmerman, Compressive strength of plain concrete under multiaxial loading conditions, ACI Material Journal (1970) 802–807.
[21] P. Launay, H. Gachon, Strain and ultimate strength of concrete under triaxial stress. Concrete for nuclear reactors, ACI SP-34-63 (I) (1972) 269–282.
[22] K.H. Gerstle, et al., Behavior of concrete under multiaxial stress states, Journal of ASCE EM6 (Dec. 1980) 1383–1403.